Laser Beam Welding of Austenitic-Ferritic Transition Joints

Weld zone constitution is compared to that predicted according to the Schaeffler estimation of phases

BY S. MISSORI AND C. KOERBER

ABSTRACT. Transition joints between austenitic stainless steels and ferritic low alloy steels are extensively utilized in many high-temperature applications in energy conversion systems. Problems related to the use of such dissimilar metal welds (DMWs) have long been recognized, because of premature failures often occurring during service, connected to thermal stresses generated at the weld interface and to metallurgical changes (carbon migration, carbide precipitation) observed after prolonged exposure to high temperature.

This paper reports the results of an investigation on DMWs carried out on plates and tubes by a deep penetration laser beam welding (LBW) process, within the framework of researching innovative welding procedures to allow for a better control of metallurgical changes and a minimization of thermal stresses.

The experimental work included metallographic observations, hardness tests, x-ray diffractometry and estimation of phases on melt zones. These data are compared with the evaluation given by the Schaeffler diagram. The results show the possibility of obtaining chemical compositions and phases according to predictions. In most instances, the melt zone constitution was close to the desired one. Further trials with filler metal of more proper composition are in progress, to improve the soundness of the joint and to optimize structure of the melt zones.

Introduction

Transition joints between austenitic stainless steels and ferritic low alloy steels are extensively utilized in many high temperature applications in energy conversion systems. In central power station boilers for economic considerations, parts such as primary tubing, operating at moderate temperatures, are made of low alloy Cr-Mo ferritic steels. On the other hand, the superheaters and the reheaters, submitted to higher temperatures, are made of austenitic stainless steel tubes. Thus, transition welds are needed. A steam boiler in a power plant can contain thousands of these joints operating at 500–550°C (932–1022°F) with a service pressure of about 16–20 MPa. Transition joints are also used in the main steam lines of power plants, in nuclear reactors, and in petrochemical plants.

Another case of dissimilar welds is encountered in welding clad plates, widely used in the construction of vessels and heat exchangers for several industrial applications. Here a structural material (carbon or low alloy steel), clad by an alloyed material (e.g., stainless steel), needs to be welded, maintaining the continuity of the cladding layer and its resistance to corrosion.

Problems related to the use of such dissimilar welds have been long recognized, because failure can occur before design life of the plant is achieved (Ref. 1). Investigations have highlighted the role of the large thermal stresses generated at the interface of weld metal-ferritic steel due to the difference in thermal expansion during temperature fluctuation. Moreover, localized metallurgical changes (carbon migration, carbide precipitation) have been observed after prolonged exposure to high temperature, thus rendering the above said interface zone more susceptible to failure. Almost all proposed failure mechanisms focused the influence of the creep damage in the carbon-depleted weakened zone, aided by the fluctuating stresses and the oxidation of ferritic steel (Refs. 2–5).

To improve the thermal behavior of dissimilar welds, research moves toward a deeper understanding of phase transformations of constituents and on innovative welding procedures and filler materials, to allow for better control of metallurgical changes and minimization of thermal stresses (Refs. 6–8).

This paper reports the results of an investigation on DMWs, carried out on plates and tubes by LBW process.

KEY WORDS

Laser Beam Welding
Dissimilar Metals
Austenitic Stainless
Cr-Mo Ferritic Steel
X-ray Diffractometry
Weld Zone Structure
Ni-Cr-Fe Filler Metal
Ferrite Content
Schaeffler Diagram
Solidification Cracking

Experimental Work

Materials and Welding Procedures

Welding trials were performed on plates and tubes. The characteristics of the materials to be welded are shown in Table 1.

In order to provide a proper welding technique it is to be considered that the weld metal derives from the fusion of the filler metal and a portion of the two dissimilar metals, according to the dilution given by the welding process utilized. The weld metal should not contain structures that may develop undesirable brittleness or cracking. As experienced with conventional welding procedures (Refs. 1–4), the best results

S. MISSORI is with Dipartimento Ingegneria Meccanica, Università di Roma-Tor, Vergata, Italy. C. KOERBER is with Fraunhofer Institut für Lasertechnik—ILT, Aachen, Germany.

Table 1 — Characteristics of Base Metals

Type	Specification	Size	Composition									Tensile strength
		mm	C	Mn	Si	P	S	Cu	Ni	Cr	Mo	MPa
2.25Cr-1Mo Ferritic Steel normalized and tempered	Plate ASTM A 387 Gr.22Cl.2	10 thick	0.118	0.48	0.241	0.014	0.018	0.27	0.194	2.170	0.93	669
	Tube ASTM A 335 Gr. P 22	Ø48x7	0.120	0.43	0.36	0.010	0.005	—	—	2.200	0.920	620
Austenitic stainless steel 18 Cr-8 Ni low carbon	Plate DIN 17740 X2 CrNi 1911	10 thick	0.018	1.15	0.41	0.025	0.001	—	10.10	18.40	—	559
	Tube DIN 17546 X2 CrNi 1911	Ø48x7	0.013	1.00	0.42	0.024	0.021	—	10.13	18.26	—	552

can be obtained with one of the following two types of filler metals:

1) Austenitic stainless steel filler metal

In this case the composition is chosen so as to obtain a predominantly austenitic weld metal, as free as possible from martensite (which might give rise to cold cracking in the weld) with little delta ferrite (which is useful to prevent hot cracking in the austenitic matrix). The typical desired composition corresponds to Type 308. It is known that an austenitic stainless steel deposit exhibits different solidification modes. With a composition close to Type 308, reference is commonly made either to primary austenite mode or to primary ferrite mode. When solidification occurs as austenite, the microstructure can be either fully austenitic or contain a little amount of ferrite along solidification grains and subgrain boundaries. When primary solidification occurs as delta ferrite, much of the ferrite transforms to austenite by a solid-state reaction during cooling to ambient temperature, but a certain amount of ferrite is retained. Hot cracking resistance is believed superior in ferrite solidification mode (Refs. 9–12). The ratio Cr_{eq}/Ni_{eq} is the main factor influencing the solidification mode; a primary ferritic solidification mode should occur when the ratio Cr_{eq}/Ni_{eq} is greater than a critical value, estimated by several studies (Refs. 13–16) in the range 1.5–1.7.

2) Nickel-Based Alloys

In this case, provided that the dilution with base materials is moderate, a fully austenitic structure in the range of Fe-Ni-Cr alloys can be obtained. The propensity toward hot cracking is associated with the formation of low melting eutectics (*e.g.*, with P, S and B), that segregate at the grain boundaries under tensile thermal stresses. This tendency can be reduced by adopting proper precautions, such as restriction of the P, S, B contents, control of Si/C ratio, low restraint conditions, good cleaning from contaminants, etc. (Refs. 17, 18). On the other hand, the solubility of carbon in this weld metal is lower than in the stainless steel, which minimizes carbon migration from the ferritic steel to the weld metal during welding and while in service. Nickel based alloy can also tolerate dilution with low alloy steel without becoming crack sensitive and, finally, its thermal expansion coefficient is much lower than stainless steel, which reduces thermal stresses at the interface between weld metal and ferritic steel. Thus, whenever the elevated temperature application demands a better performance in terms of creep and fatigue resistance, nickel based filler materials are recommended to achieve a longer service life (Refs. 3, 4).

According to these metallurgical reasons, we utilized in our work the two types of filler material as reported in Table 2, consisting of an austenitic stainless steel Type 309 (24% Cr, 13% Ni) and a nickel alloy (about 70% Ni). After a number of preliminary trials, it was decided to utilize the welding procedures with the parameters shown in Table 3. Filler material is put into the joint in the following different ways:

1) austenitic stainless steel filler metal as conventional welding wire 0.8 mm diameter (0.032 in.) for procedures I-A, I-B;

2) austenitic stainless steel filler metal as N.4 x 0.4 mm (0.016 in.) strips, 1.6 mm (0.064 in.) total thickness, procedure II-A, II-B) or N.5 x 0.4 mm strips, with 2.0 mm (0.08 in.) total thickness, procedure III-A, III-B;

3) nickel-based filler metal, as N.4 x 0.4 mm strips (1.6 mm total thickness) for procedure IV-A, IV, or N.5 x 0.4 mm strips (2.0 mm total thickness), for procedure V-A, V-B.

Welding assemblies and the edge preparations for plates and tubes are reported in Fig. 1. In the case of strip filler metal, the strips were interposed between the edges and fixed by gas tungsten arc welding (GTA) tack-welding before laser beam welding.

The laser welding equipment was a CO_2 unit, UT 25 kW, DC, with an unstable resonator multimode configuration, linearly polarized. The optical device was an 18.75-in. (476-mm) SPAWR optic, consisting of a cylindrical bending mirror and a spherical focusing mirror. Control of plasma was obtained by using a transverse stream of helium. The gas nozzle had an inner diameter of 4 mm (0.16 in.) and was directed just above the interaction zone of beam and workpiece. Before welding a diagnostic system was utilized to check the characteristics of the laser beam; the Rayleigh length, calculated on the basis of beam diagnostic, was comparable with the thickness of workpieces.

Neither preheat nor postweld heat treatment was utilized.

Examinations and Tests

After completion, each of the weld joints was submitted to the following

Table 2 — Characteristics of Filler Metals

N	Specification	Shape	C	Mn	Cr	Si	Ni	Mo	Nb	Fe
1	AWS ER 309L	wire Ø 0.8 mm	≤0.025	1.70	24.0	0.80	13.0	—	—	bal.
2	AWS E 309 L	strip 0.4 mm thick	0.010	1.65	24.5	0.33	12.4	0.47	—	bal.
3	AWS E Ni Cr3	strip 0.4 mm thick	0.020	3.00	20.5	0.10	bal.	—	2.5	1.5

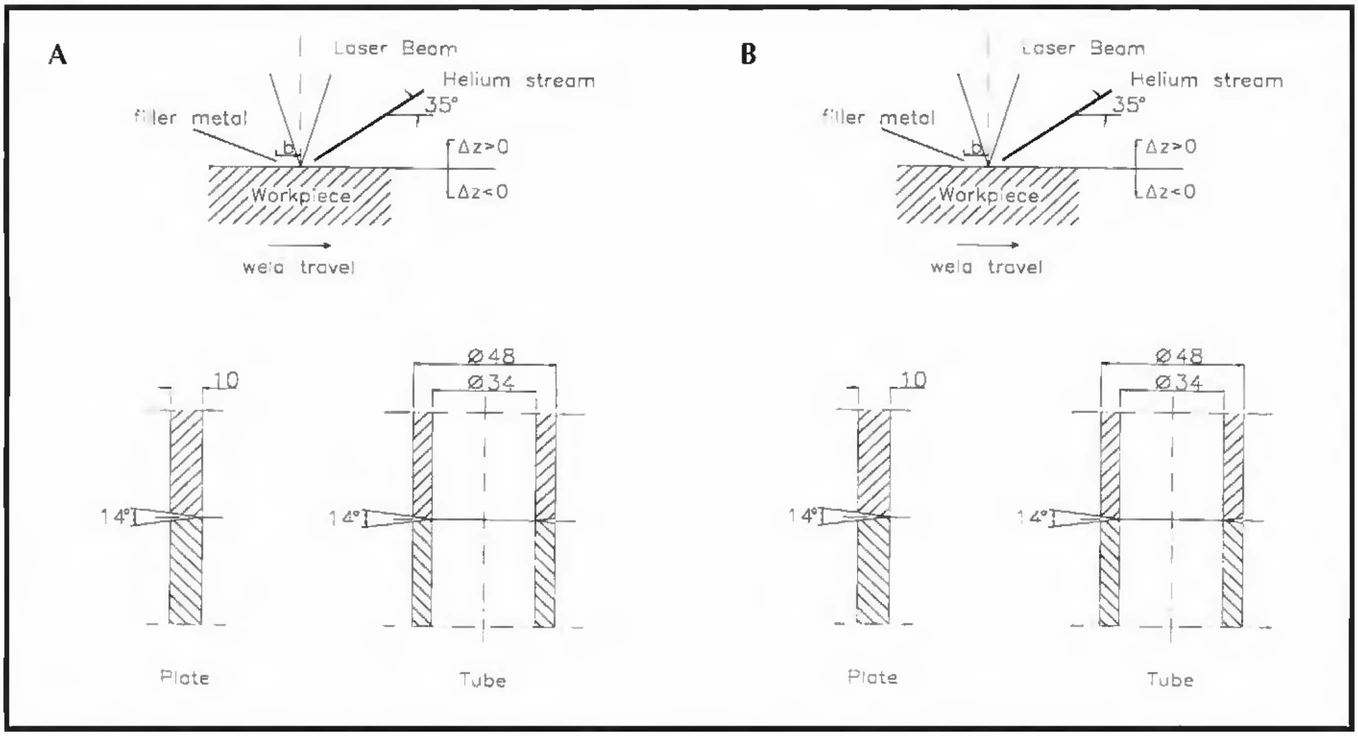

Fig. 1 — Welding assemblies and edge preparations: A — I–A (plate), I–B (tube); B — II, III, IV, V–A (plate), –B (tube).

examinations and tests: visual inspection, radiographic and macrographic examination, tensile tests; x-ray diffractometry; measurement of areas of welds and estimation of weld deposit microstructures; metallographic examination and microhardness tests.

Results

Inspections

All welds were submitted to visual inspection; at least three macrographic samples per each procedure were cut and examined. Moreover, all welds coming from plates underwent a complete radiographic inspection. The results of this inspection can be summarized as follows (see macrographs on Figs. 2A–I): samples I-A and I-B show satisfactory appearance at visual and macrographic examination; radiographic inspection of welds on plates was satisfactory; samples II-A, II-B, III-A show some incomplete fusion at root, stainless steel side; no other remarkable defects on the sound portion of the welds has been revealed by visual and radiographic examination; sample III-B shows lack of penetration at austenitic steel side (not reported in the figure); samples IV-A, V-A, IV-B, V-B show some occasional incomplete penetration at the root side; some minor porosity was revealed at the macrographic and radiographic examination; the class of quality was acceptable according to category B of DIN 8563 T.11.

Tensile Tests

In order to test the mechanical strength of welds, N.2 tensile tests were performed from each of three welded

Table 3 — Welding Parameters

Welding procedures for plates	I-A	II-A	III-A	IV-A	V-A
Power at the workpiece, kW	9	14	14	14	14
Number of passes	2	1	1	1	1
Welding speed, m/min (in./min)	1.0 (39.3)	1.4 (55.1)	1.4 (55.1)	1.4 (55.1)	1.4 (55.1)
Wire feeding speed, m/min (in./min)	10 (393)	—	—	—	—
Power density, MW/cm^2 (MW/in.^{2})	0.438	0.681 (4.39)	0.681 (4.39)	0.681 (4.39)	0.681 (4.39)
Filler metal composition and size: by Table 2	1	2	2	2	3
Shape	wire	N.4 strips	N.5 strips	N.4 strips	N.5 strips
Position per ASME IX			Horizontal (2G)		
Welding procedures for tubes	**I-B**	**II-B**	**III-B**	**V-B**	**V-B**
Power at the workpiece, kW	10	10	10	10	10
Welding speed, m/min(in./min)	1.6 (63)	1.6 (63)	1.6 (63)	1.6 (63)	1.6 (63)
Wire feeding speed, m/min (in./min)	8.0 (315)	—	—	—	—
Power density, MW/cm^2(MW/in.^{2})	0.487 (3.14)	0.487 (3.14)	0.487 (3.14)	0.487 (3.14)	0.487 (3.14)
Filler metal composition and size: by Table 2	1	2	2	2	3
Shape	wire	N.4 strips	N.5 strips	N.5 strips	N.5 strips
Position per ASME IX			Horizontal (2G)		

Note: The helium flow rate for all procedures is 25 L/min (53 cfh). Tubes are welded with a single pass in all cases.

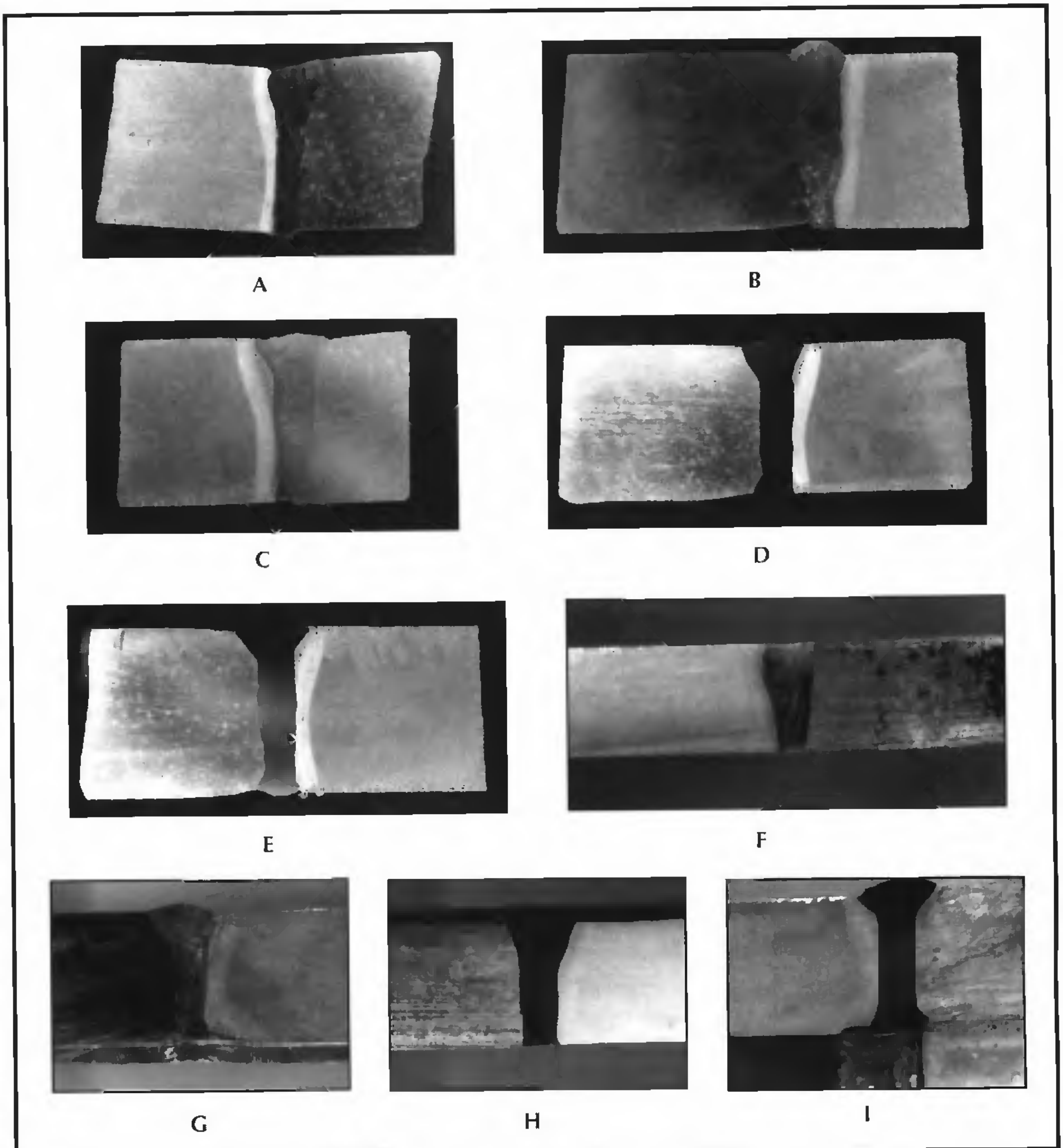

Fig. 2 — Macrographs of cross section of welds (2.5X): A — I-A; B — II-A; C — III-A; D — IV-A; E — V-A; F — I-B; G — II-B; H — IV-B; I — V-B.

joints assumed as representative of the three ways of formation of the weld zone, that is with filler metal Type 309 as wire (sample I-A), Type 309 as strip (sample III-A) and nickel-based as a strip (sample IV-A). All values obtained for procedure I-A were satisfactory (failure located on base metal, stainless steel side) and are reported in Table 4. Instead, tests on specimens welded with strip filler metal (sample III-A, IV-A) resulted in premature failure due to the occasional occurrence of incomplete fusion on tensile specimens.

X-ray Diffractometry of the Weld Zones

X-ray diffractometry analysis (XRD) was carried out to investigate phases present in the melted zones on samples taken from joints from plates (one sample per each procedure). Mo $K\alpha_1$ radiation ($\gamma = 0.71$ Å) was used. Each sample was cut so that a longitudinal middle cross section of the weld, representative of the fusion zone, was submitted for analysis. The XRD patterns of samples coming from procedures I-A, II-A, III-A show a double set of diffraction lines revealing the presence of the two phases α and γ.

Instead, the patterns of samples from procedures IV-A and V-A show a single set of lines corresponding to the presence of phase γ only. The relative amounts of the phases α and γ have been estimated from the integrated intensities of diffraction lines. The results are reported in Fig. 3 and Table 5.

Microhardness Test

Several metallographic specimens were machined from each weldment. Microhardness tests were performed by measuring values along a line located in the middle of the thickness and crossing both heat-affected zones and fusion metal. The Vickers test was used with a load of 100 g_f and a loading time of 10 s — Fig. 4A–E.

Microstructure Estimation According to Schaeffler Diagram

The Schaeffler diagram was used to estimate the microstructure of the weld zones for samples taken from plates. The survey of the dimensions of each cross section of the welds was performed with the aid of an optical microscope, by measuring the width of the melt zone at several points moving along the centerline of the weld zone — Fig. 4A–E. Weld sections were drawn and the areas were calculated with the help of a CAD program. Taking into account the composition of base and filler materials and the quantity of filler material added into the weld zone, the equivalent values of Cr and Ni were evaluated. The two base metals were supposed to give an equal contribution to the weld zone. After evaluation, the points representing the microstructures for the various procedures were reported on the Schaeffler diagram — Fig. 5.

Metallographic Examination

Microstructures on the Ferritic Steel HAZ

The ferritic steel 2.25 Cr-1 Mo is supplied normalized at 920°C (1688°F) and tempered at 730°C (1346°F). The former treatment gives rise to the formation of bainite mixed to martensite, the latter transforms such a structure to ferrite with dispersed carbides (HV ≅ 220) — Fig. 6.

During welding, the region close to the fusion line undergoes a fast heating at a temperature exceeding the point Ac_3 (transformation ferrite→austenite). Microstructural changes occurring in the HAZ at the ferritic steel side depend on the kinetics of formation of austenite and its grain size, according to the Continuous Cooling Transformation (CCT) diagram of the steel (Ref. 19). It is well known that the closer the distance to the fusion line is, the higher the peak temperature and the hold time at elevated temperature are. In the case of a single-pass weld, it is possible to foresee the formation of three zones:

1) a first zone where the austenite developed during heating over Ac_3 giving rise to a mixed martensite-bainite structure with a coarse grain, favored by time and temperature conditions;

2) a second zone where the austenite developed at lower temperature and the resulting structure is a more fine-grained bainite + martensite;

3) a third zone where the temperature is raised to a value between Ac_1 (start of austenitic transformation) and Ac_3, with partial austenitization and formation during cooling of a mixture of transformation structures of prior austenite and untransformed material.

Metallographic analysis confirmed this expectation. With reference to a

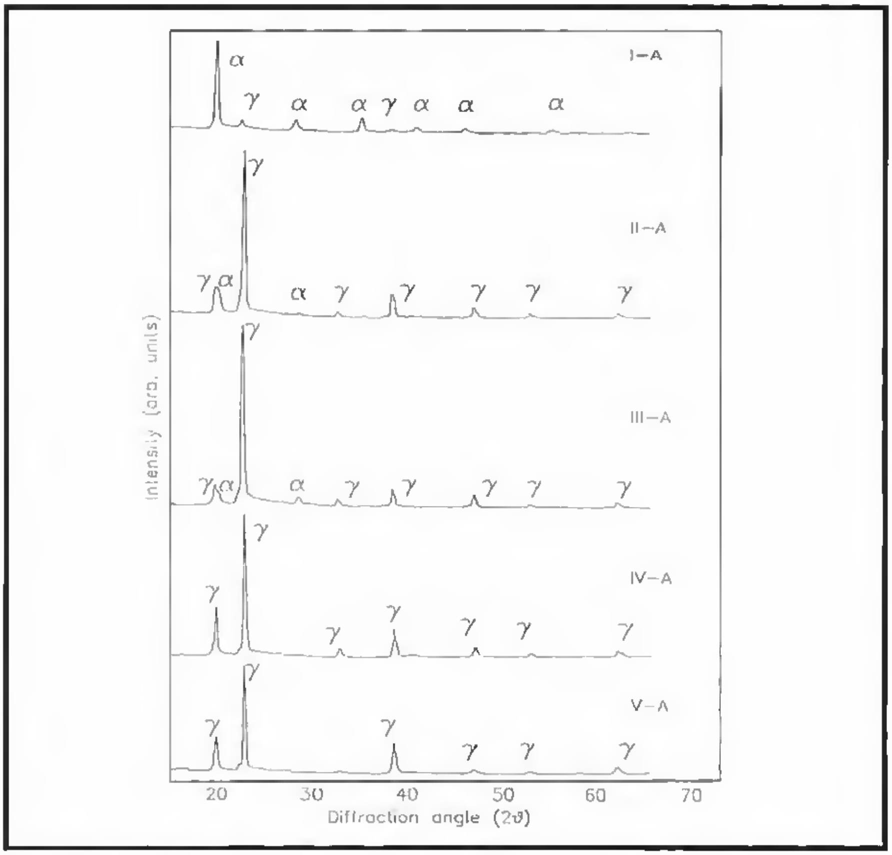

Fig. 3 — X-ray diffractometer analysis for weld zone with procedures I, II, III, IV, V-A.

Table 4 — Tensile Tests

Specimen	Welding procedure	Tensile strength (MPa)	Failure location	Distance from weld zone
1	I-A	607	Base metal, stainless steel side	15 mm
2	I-A	603	—	13 mm

Table 5 — X-ray Diffraction Analysis

Sample	Welding procedure	Estimated amounts of phases %	
		α	γ
1	I-A	73	27
2	II-A	11	89
3	III-A	8	92
4	IV-A	0	100
5	V-A	0	100

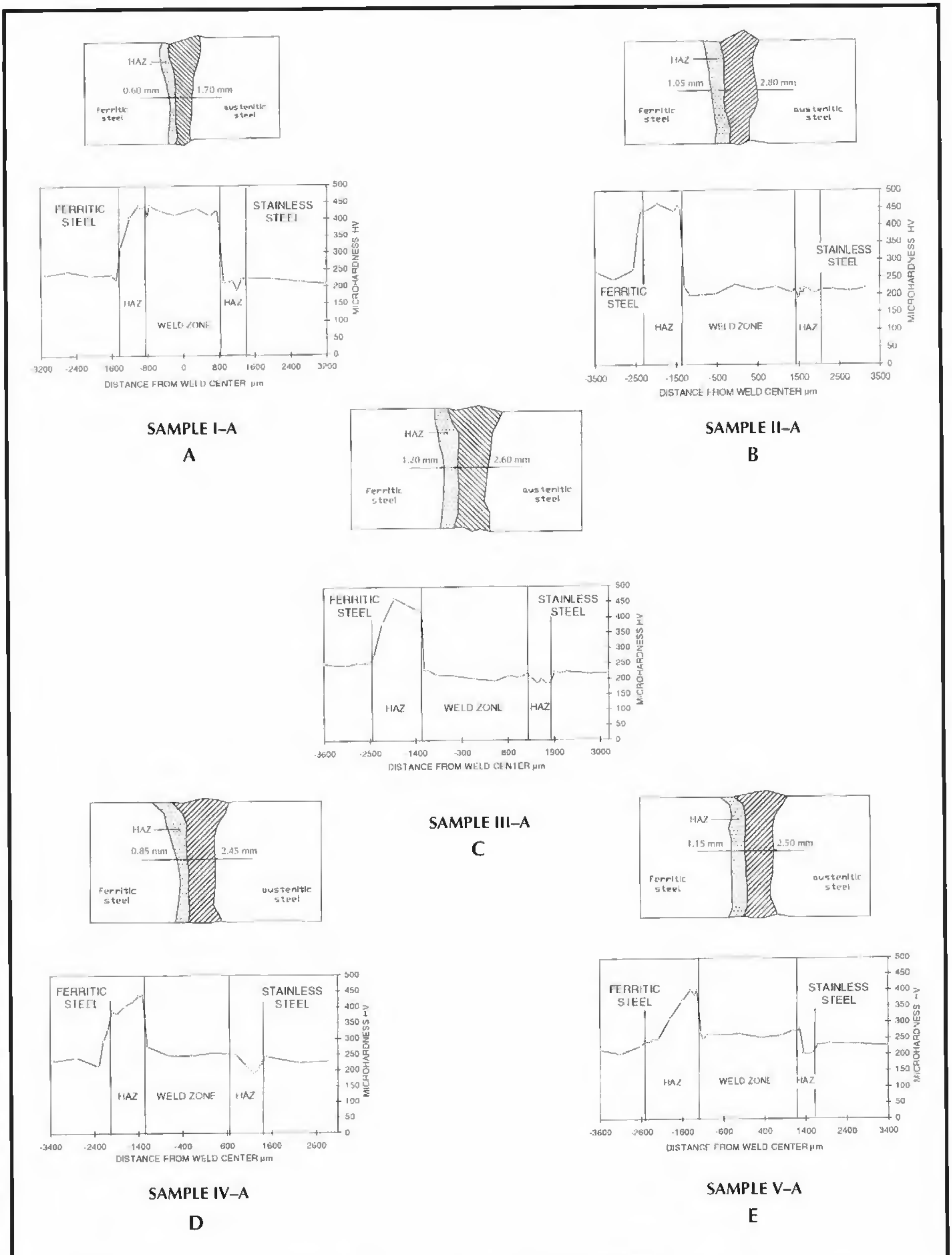

Fig. 4A–E — Microhardness tests and measured cross sections of welds.

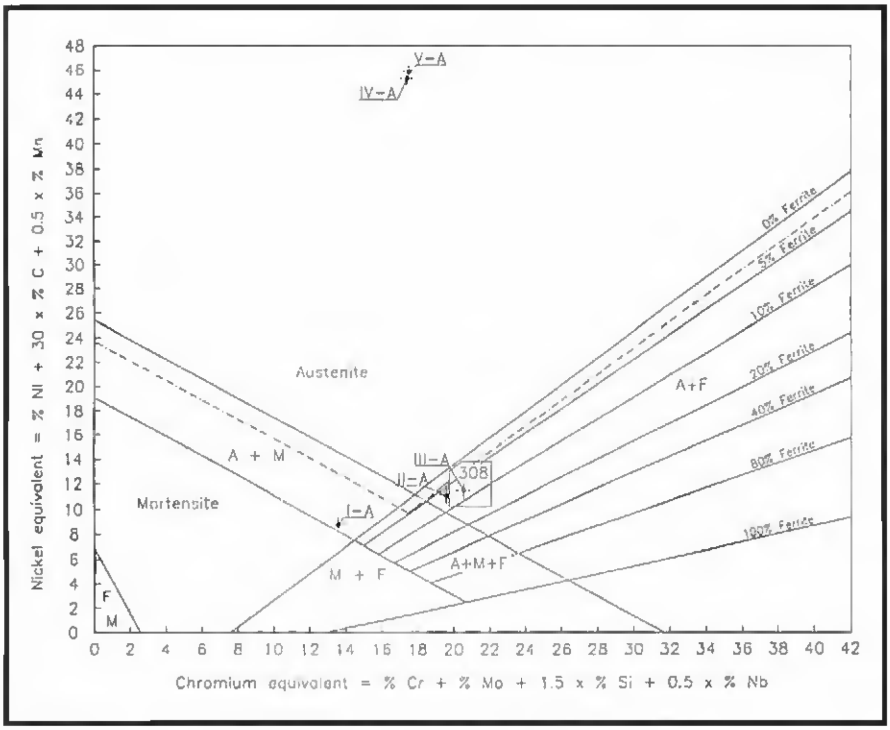

Fig. 5 — Estimation of weld zone phases on the Schaeffler diagram.

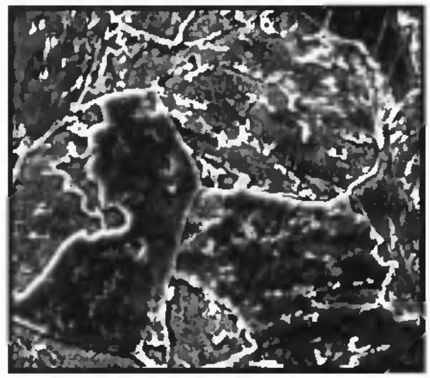

Fig. 6 — SEM micrograph of the microstructure of ferritic steel as-supplied, etched with nital: ferrite with dispersed carbides (2000X).

specimen welded with procedure IV-A (assumed as representative), the HAZ has a total width of ≈ 1 mm (Fig. 7A) and is characterized by: a first zone, about 0.2 mm wide, in which needle-like martensite, probably mixed to bainite, (Fig. 7B) with a microhardness of HV = 400–450 can be observed; a second zone, about 0.4–0.5 mm wide, in

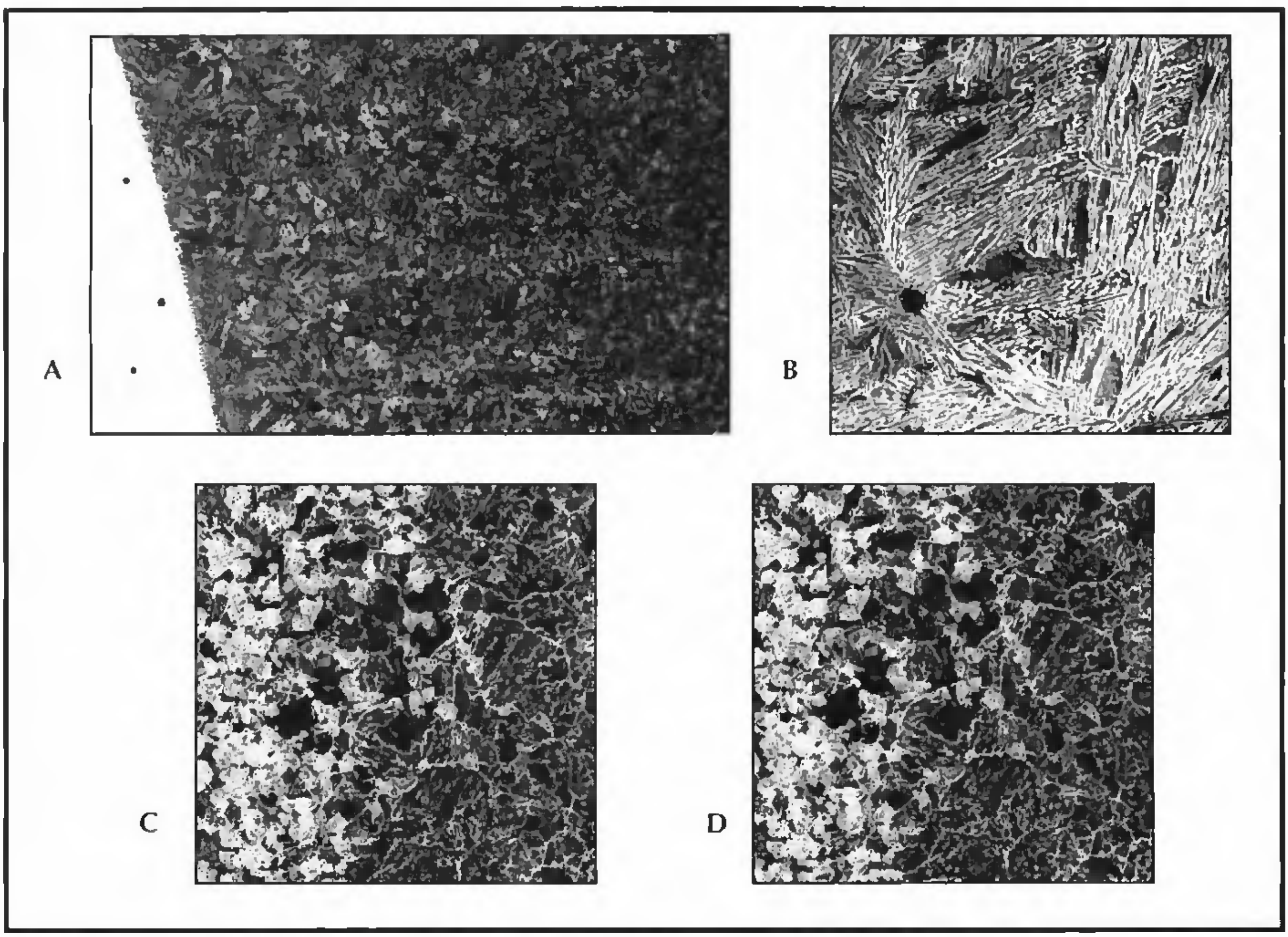

Fig. 7 — Microstructure of ferritic steel HAZ, etched in nital: A — overall view (200X); B — SEM micrograph of zone near the weld interface, coarse-grained, ≈ 0.2 mm wide, HV = 437 (1000X); C — SEM appearance of the transition zone between HAZ and unaffected microstructure at 1 mm of distance from weld interface (500X), HV = 300–350; D — detail of the transition zone in C (2600X).

which martensite mixed to bainite is more fine-grained, with still elevated values of microhardness (HV = 410–460); a third zone (Fig. 7C, D), partially austenitized, in which the transformed structures of prior austenite are delimiting parts of untransformed ferrite (HV = 300–350).

Microstructures of Weld Metal Zones

The estimation according to the Schaeffler diagram and the results of x-ray examination suggest the formation of the following three basic types of microstructures of weld zones:

1) martensitic with some austenite for procedures I-A/B;

2) austenitic with some delta ferrite for procedures II-A/B, III-A/B;

3) fully austenitic (nickel alloyed) for procedures IV-A/B, V-A/B.

Metallographic observations, validated by the results of microhardness tests, are in accordance with this evaluation: samples welded with austenitic wire filler metal show a structure mainly consisting of coarse and massive martensite with a microhardness HV ≅ 420 — Fig. 8A; samples welded with austenitic strip filler metal show an austenitic matrix with delta ferrite of the vermicular (skeletal) type, with a dark etching appearance, HV ≅ 205 — Fig. 8B; samples welded with nickel-based filler metal show a fully austenitic structure having a cellular pattern, with the presence of little porosity, HV ≅ 260 — Fig. 8C.

Microstructure in Austenitic Steel HAZ

Microstructure on the austenitic steel close to the weld interface shows a little alteration after welding, revealed by a slight decrease in microhardness (about 20–30 HV) in a narrow band, 0.5–0.7 mm wide. In this zone, a recrystallization of grains, deformed because of high residual stresses arising from heat treatment of the steel (solution annealing with fast cooling), is likely to occur. Metallographic observation (Fig. 9) allowed identification of the presence of small recrystallization grains, which could be responsible for this softening in the zone reaching a temperature high enough (likely to be over 700–900°C [1292–1652°F]) to induce it.

According to expectation (austenitic steel is of low-carbon type), no precipitation of carbides was revealed at the metallographic observation.

Discussion

In general, the experimental results demonstrated the possibility of producing deep penetration welds with the LBW process, by minimizing thermally induced distortion and residual stresses, thanks to the smaller size of the weld zone, if contrasted with conventional welding processes. For comparison, in a welding trial of a plate 10 mm thick, welded with manual arc procedure in six passes, the melt zone width was variable within 5 and 15 mm, and the ferritic steel HAZ was 2–3 mm wide (Ref. 20). In the present cases with LBW, the melt zone width was reduced to ≈ 2–3 mm and the ferritic steel HAZ became ≈ 1 mm wide.

Procedures with Wire Filler Metal

The samples from procedures I-A and I-B (with wire austenitic filler metal) exhibited a good mechanical soundness and satisfactory macrographic/radiographic appearance. The estimated composition (Cr_{eq}=13.5, Ni_{eq}=8.7), however, was quite far from the desired one (this latter being represented in the Schaeffler diagram within the range of Type 308 weld metal). The reason why the weld zone resulted lean in Cr and Ni is connected to the composition of filler material (not adequate content), or to low wire feeding speed, or to low wire diameter. From the results of x-ray diffractometry and metallographic observation, a predominant presence of martensite has been assessed. The estimated content of the martensitic phase is about 73%, the remaining 27% being retained austenite. This is also validated by the high value of hardness (HV = 420), recorded in the weld metal. Although an accurate inspection on several sections was performed, no cracks were detected in the weld, possibly associated with the tendency toward cold cracking of the martensitic phase.

Procedures with Strip Filler Metal

In the case of austenitic stainless steel melt zones (samples II-A/B, III-A/B), numerous earlier studies on the solidification zones highlighted the cracking susceptibility of welds with a composition similar to Type 308. It is generally recognized that the solidification

Fig. 9 — Overall view (200X) of microstructure of austenitic stainless HAZ, etched in glyceregia, in sample V-A. HAZ is subject to a softening for a width of about 0.5 mm, HV = 200.

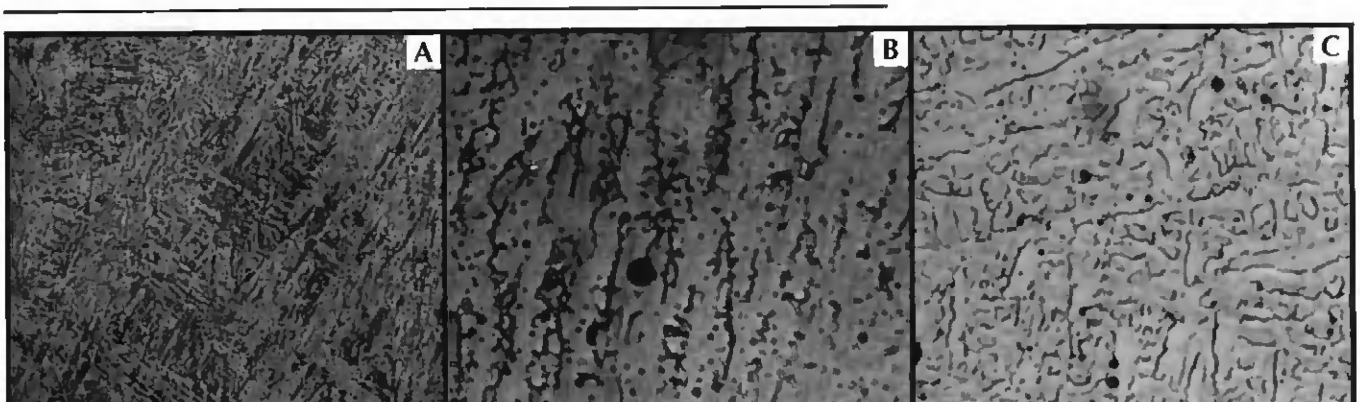

Fig. 8 — Microstructure of weld metal zones, etched in glyceregia: A — martensitic microstructure in sample I-A (Type 309 filler wire), HV = 420 (500X); B — austenitic matrix with some delta ferrite in sample II-A (Type 309 filler metal strips), HV = 205 (500X); C — austenitic nickel alloyed matrix in sample IV-A (nickel-alloy filler metal strips), HV = 260 (500X).

mode is the main factor dictating whether crack-free welds can be produced. If delta ferrite is the primary solidification product, welds are more resistant to cracking than alloys of similar composition, which solidified with austenite as the primary product. Generally, a presence of ferrite above 5% results in primary ferrite solidification mode. In our cases, the content of α-phase as delta ferrite, estimated by x-ray diffractometry, is 8% and 11%, respectively, for samples II-A/B and III-A/B. This is also confirmed by the evaluation on the Schaeffler diagram and by the metallographic observation of the weld zone, which generally show an austenitic matrix with a the presence of ferrite of the vermicular (skeletal) type, with a dark etching appearance. The morphology of this ferrite suggests that primary ferrite solidification mode has predominantly occurred. No cracks were observed either metallographically or by x-ray inspection. This result is consistent with the principle that Type 308 stainless steel welds are resistant to hot cracking when solidified as primary ferrite.

In the case of nickel-based filler metal (samples IV-A/B, V-A/B), a fully austenitic structure has been obtained in accordance with metallographic observations and x-ray diffractometry. The estimated composition on the Schaeffler diagram is approximately within the range of the weld metal Type 330. No cracks were observed either metallographically or through x-ray inspection, but only the presence of a little porosity.

Incomplete fusion, occasionally encountered in a portion of the thickness at the root side, has been attributed to the particular shape of the filler metal, consisting of a number of thin packed strips, which is known to be unfavorable to the heat flow toward the base metal (due also to the low thermal conductivity of the austenitic phase). Some spots of lack of fusion occasionally resulted in the base metal at root side; in the welding trial conditions, the total thickness of the strips resulted very near to the maximum width of the obtained melt zone. On the other hand, a relatively high number of strips was necessary to meet the metallurgical demand to achieve an adequate alloy element content (in particular Cr and Ni), to compensate for dilution with ferritic low-alloy steel. This experimental result suggests that, in future trials, it would be convenient to reduce the thickness of the filler strip, by increasing the alloy content in Cr and Ni, in order to compensate for the consequent greater dilution from base metals (weld width being equal), in particular from low-alloy ferritic steel.

Conclusions

Even though further trials are required, preliminary results confirmed the possibility of carrying out successfully DMWs by the LBW process, taking advantage of peculiar features of the LBW process. The main advantages are the area reduction of melted zone and HAZ, and the consequent minimization of distortion and residual stresses induced by heat input on workpieces, when contrasted with conventional welding processes. Moreover, the LBW process allows a single-pass full-penetration welding technique.

For optimization of the procedure I-A/B (with filler wire), it will be necessary to reduce the elevated hardness in the weld zone by moving its composition toward the austenitic phase and decreasing the martensite content. This may be accomplished by increasing the alloy content in Cr/Ni, so as to approach the desired composition Type 308.

The main problem encountered with procedures using a strip filler metal was the achievement of a complete weld fusion at the root side. This was attributed to poor heat transfer through the packed filler strips of austenitic filler metal, having even lower thermal conductivity. The total thickness of the strips, assessed to fulfill the metallurgical demand on the weld structures, resulted very nearly to the maximum width of the melted zone in the trial conditions. In some of the observed cases, the complete fusion at the root side was not achieved on one edge. This difficulty could possibly be overcome in future trials by utilizing one integral strip, with a reduced thickness, *e.g.*, down to 1 mm (0.04 in.), instead of a number of the strips; the metallurgical requirement could be fulfilled with the use of more alloyed filler materials (not readily available at present), especially provided for the LBW process, either of nickel-based or austenitic stainless steel types. For instance, according to our evaluation, if a weld zone Type 308 is desired, the filler material should have a composition higher alloyed in Cr than the Type 309 utilized so far (up to approximately $Cr_{eq} = 35\%$, $Ni_{eq} = 18\%$, with a Cr_{eq}/Ni_{eq} ratio of about 2.0), in order to compensate for the dilution with ferritic steel.

A final consideration on utilization of either wire or strips as filler material can be made. It is well known that consumable inserts of several configurations (inverted T, Y, rectangular shape, etc.) are often employed with conventional arc welding for better fit-up and easier root welding of components that cannot be back welded from inside (*e.g.*, piping). In these cases, LBW with filler strips appears a natural and convenient choice. On the other hand, in the case of welding on large-diameter components, the use of filler wire could be preferable, as it allows for easier and more economical preparation of the joint.

Acknowledgments

This work was supported by the *Human Capital and Mobility Program* of the European Community within the framework of the project *European Laser Center* at the Fraunhofer Institut für Lasertechnik in Aachen, Germany. Thanks to ESAB for providing filler materials.

References

1. Lundin, C. D. 1982. Dissimilar metal welds — literature review. *Welding Journal* 61 (2): 585-s to 635-s.

2. Hardy, A. K., and Rowley, T. 1978. Austenitic/ferritic welded transition joints for high temperature application. *Ferritic steels for fast reactor steam generator*, British Nuclear Energy Society, London, England, pp. 481–487.

3. Viswanathan, R. 1985. Dissimilar metal welds in service and boiler creep damage evaluation for plant life extension. *Journal of Pressure Vessels Technology*, Vol. 107, pp. 218–225.

4. Roberts, D. I., Ryder, R. H., and Viswanathan, R., 1985. Performance of dissimilar welds in service. *Journal of Pressure Vessels Technology*, Vol. 107, pp. 247–254.

5. Brutti, C., Gauzzi, F., and Missori, S. 1992. Life prediction and microstructures of dissimilar metal welds. *Proc. of the III Internat. Confer. on Low Cycle Fatigue and Elastoplastic Behaviour of Materials*, Berlin, Germany, pp. 671–677.

6. Klueh, R. L., and King, J. F. 1982. Austenitic-ferritic weld-joint failures. *Welding Journal* 61 (9): 302-s to 311-s.

7. King, J. F., Sullivan, M. D., and Slaughter, G. M. 1977. Development of an improved stainless steel to ferritic steel transition joint. *Welding Journal* 56 (11): 354-s to 358-s.

8. Missori, S., and Sili, A. 1992. Austenitic-ferritic transition joints welded by buttering technique. *Applications of Stainless Steels '92*, Vol. 2, Jernkontoret, Stockholm, Sweden, pp. 986–992.

9. Singh, J., Purdy, G. R., and Weatherly, G. C. 1985. Microstructural and microchemical aspects of the solid-state decomposition of delta ferrite in austenitic stainless steels. *Metallurgical Transactions A*, 16A (8), pp. 1363–1369.

10. Kujanpaa, V. P., David, S. A., and White, C. L. 1986. Solidification cracking, formation of hot cracks in austenitic stainless steel welds. *Welding Journal* 65 (8): 203-s to 212-s.

11. David, S. A., Vitek, J. M., and Hebble, T. L. 1987. Effect of rapid solidification on stainless steel weld metal microstructures and its implications on the Schaeffler diagram. *Welding Journal* 66 (10): 289-s to 302-s.

12. Vitek, J. M., and David, S. A. 1988. The effect of cooling rate on ferrite in Type 308 stainless steel. *Welding Journal* 67 (5): 95-s to 102-s.

13. Kujanpaa, V., Suutala, N., Takalo, T., and Moisio, T. 1979. Correlation between solidification cracking and microstructure in austenitic-ferritic stainless steels welds, *Welding Research Intl.*, 9 (2): pp. 55–70.

14. Lundin, C. D., Chou, C. P. D., and Sullivan, C. J. 1980, Hot cracking resistance of austenitic stainless steel weldments. *Welding Journal* 59 (8):226-s to 232-s.

15. Lippold, J. C. 1985. Centerline cracking in deep penetration electron beam welds in Type 304L stainless steel. *Welding Journal* 64 (5): 127-s to 136-s.

16. Lippold, J. C. 1994. Solidification behavior and cracking susceptibility of pulsed-laser welds in austenitic stainless steels. *Welding Journal* 73 (6): 129-s to 143-s.

17. Arata, Y., Matsuda, F., and Katayama, S. 1977. Solidification crack susceptibility in weld metals of fully austenitic stainless steels. *Transactions JWRI* (6) 1: pp. 105–116.

18. Cieslak, M. J., Headley, T. J., and Frank, R. B. 1989. The welding metallurgy of custom age 625 PLUS alloy. *Welding Journal* 68 (12): 473-s to 482-s.

19. Schrader, A., and Rose, A. 1966. *De Ferri Metallographia*, Verlag Stahleisen GMBH, Düsseldorf, Germany, p. 127.

20. Gauzzi, F., and Missori, S. 1988. Microstructural transformations in austenitic-ferritic transition joints. *Journal of Material Science*, 23, pp. 782–789.